Prandtl number effects in decaying homogeneous isotropic turbulence with a mean scalar gradient

Antoine Briard, Thomas Gomez

Journal of Turbulence
Vol. 18, No. 5, pp: 418-442, 2017, 1–23

RESEARCH ARTICLE

Prandtl number effects in decaying homogeneous isotropic turbulence with a mean scalar gradient

A. Briard[a] * and T. Gomez[b]

[a]*Sorbonne Universités, UPMC Univ Paris 06, CNRS, UMR 7190, ∂'Alembert, F-75005, Paris, France*; [b]*USTL, LML, F-59650 Villeneuve d'Ascq, France*

(*Received 00 Month 200x; final version received 00 Month 200x*)

Decaying homogeneous isotropic turbulence with an imposed mean scalar gradient is investigated numerically, thanks to a specific eddy-damped quasi-normal Markovian (EDQNM) closure developed recently for passive scalar mixing in homogeneous anisotropic turbulence [Briard et al., J. Fluid Mech. **799** (2016)] (BGC). The present modelling is compared successfully with recent direct numerical simulations and other models, for both very large and small Prandtl numbers. First, scalings for the cospectrum and scalar variance spectrum in the inertial range are recovered analytically and numerically. Then, at large Reynolds numbers, the decay and growth laws for the scalar variance and mixed velocity-scalar correlations respectively, derived in (BGC), are shown numerically to remain valid when the Prandtl number strongly departs from unity. Afterwards, the normalized correlation $\rho_{w\theta}$ is found to decrease in magnitude at a fixed Reynolds number when Pr either increases or decreases, in agreement with earlier predictions. Finally, the small scales return to isotropy of the scalar second-order moments is found to depend not only on the Reynolds number, but also on the Prandtl number.

Keywords: Homogeneous Turbulence, Scalar Gradient, Cospectrum, EDQNM

1. Introduction

The mixing of a passive scalar field in homogeneous turbulence has been the subject of many theoretical, numerical and experimental works. Despite this attention, there are still some open questions, as reviewed by Warhaft [1], notably about local isotropy of the scalar field. The return to isotropy of scalar small scales has been greatly investigated and it appears that even at moderately high Reynolds numbers, anisotropy seems to persist at small scales in shear flows [2]. Homogeneous shear flows being rather complex, it is convenient to study simpler frameworks to investigate the distribution of anisotropy at the level of the passive scalar field: decaying homogeneous isotropic turbulence with a mean scalar gradient (HITSG). Even in such a configuration where the velocity field is isotropic, persistent small scales anisotropy is often observed at the level of the third-order moments [3–5], at least at the moderate Reynolds numbers considered. Nevertheless, this is not incompatible with second-order moments being locally isotropic in HITSG [6], in agreement with a recent numerical work performed at very large Reynolds numbers [7]. It is worth noting that local isotropy was also recovered experimentally in HITSG for the scalar third-order moments [8]. The diversity of the results regarding the return to isotropy of the scalar field in HITSG illustrates that such a framework still requires some work. Since most of the avail-

*Corresponding author. Email: antoine.briard@upmc.fr

ISSN: (online only)

DOI:
http://www.tandfonline.com

able research in HITSG was performed with a Prandtl number close to unity, where Pr is the ratio of kinematic viscosity ν to scalar diffusivity a, the emphasis is consequently put here on effects of Prandtl numbers very different from unity, at large Reynolds numbers, on spectral scalings and dynamics of scalar one-point statistics.

As stated before, HITSG received some attention in the past decades both experimentally and numerically [4, 8–14]. This configuration is of particular interest in direct numerical simulation (DNS) since it is often used as a way to obtain a stationary scalar field without an artificial forcing term. Indeed, in such a configuration, the vertical mean scalar gradient $\partial\Theta/\partial x_3$ produces scalar fluctuations so that the scalar variance $K_T =< \theta^2 >$, where θ and Θ are respectively the fluctuating and mean parts of the scalar field, can increase with time, or at least balance diffusion. Whereas in HITSG, the kinetic energy $K =< u_i u_i > /2$ decreases with time, where u_i is any component of the fluctuating velocity field. Such a framework presents also the advantage that the velocity field remains completely isotropic, so that all anisotropic effects addressed are exclusively the results of the mean scalar gradient. The first effect of anisotropy, created through the mean scalar gradient, is the appearance of the mixed-correlation $< u_3\theta >$, or cospectrum in spectral space, which is of practical importance for the development and improvement of Reynolds Average Navier Stokes (RANS) models and Large Eddy Simulations (LES) subgrid models: indeed, the scalar flux is the unclosed term of the mean scalar field evolution equation. Since $< u_3\theta >$ acts as a production term for $< \theta^2 >$, it is the cause of the scalar field departure from isotropy.

Most of the papers dealing with a Prandtl number different from unity in HITSG were done at moderate Reynolds numbers, and focused on its effects on high-order scalar statistics, and on the cospectrum $\mathcal{F}(k,t)$ and scalar variance spectrum $E_T(k,t)$ spectral scalings as well [15–17]. The aim of the present study is to explore asymptotic regimes of HITSG, at very large Reynolds numbers and either very high or small Prandtl numbers, in order to predict the growth and decay rates of the scalar variance $< \theta^2 >$ and mixed-correlation $< u_3\theta >$ of highly and weakly diffusive scalars, which is a new feature, and to verify the proposed spectral scalings as well. This is of theoretical interest since these regimes cannot be reached experimentally nor in DNS yet. In addition, this permits to analyze the combined effects of anisotropy that mainly affect large scales, and Pr which dominantly modifies small scales of the spectra. Furthermore, it has been shown recently numerically, thanks to a classical eddy damped quasi normal Markovian (EDQNM) closure, that the Prandtl number did not affect the theoretical decay exponent of the scalar variance in homogeneous isotropic turbulence (HIT) [18]. Consequently, a natural extension of this work is to address effects of Prandtl numbers on the time evolution of $< \theta^2 >$ and $< u_3\theta >$ in an anisotropic framework such as HITSG at large Reynolds numbers.

In order to do so, a spectral anisotropic closure was recently developed for passive scalar dynamics, in Briard, Gomez and Cambon [7], referred to as (BGC). This closure, called *anisotropic EDQNM modelling*, is dedicated to the investigation of passive scalar mixing at large Reynolds numbers in homogeneous anisotropic turbulence (HAT), and is valid in the presence of both mean velocity and scalar gradients. The procedure of the modelling is twofold: first, the exact evolution equations of the two-point second-order spectral correlations are closed by a classical EDQNM procedure, as intensively detailed in [7, 18–20]. Then, expansions in spherical harmonics of these two-point correlations are performed, and truncated at the second order, so that anisotropy can be investigated thanks to spherically-averaged tensors which depend only on the modulus k of the wavevector $\boldsymbol{k}$. The

validation of these assumptions is done by comparisons to multiple cases with shear, distortion, mean scalar gradients, various intensities of mean gradients, and multiple Reynolds numbers in three papers [7, 20, 21]. However, in (BGC), only the case $Pr = 1$ was addressed: therein, theoretical decay and growth exponents for $< u_3\theta >$ and $< \theta^2 >$ respectively were derived for HITSG, and assessed numerically. Therefore, the present work is an application of the anisotropic EDQNM modelling when the Prandtl number strongly departs from unity, basically from 10^{-5} to 10^4. Investigating an anisotropic configuration such as HITSG at large Reynolds numbers, with either very large or small Prandtl numbers, with an approach previously validated in more complex configurations such as shear-driven flows, is an important contribution in terms of modelling.

The paper is structured as follows. In section 2, the main elements of (BGC) are recalled, notably the definitions and final evolution equations within our anisotropic EDQNM modelling framework. Initial conditions and the numerical setup are provided as well. Then, in section 3, the theoretical spectral scalings of the cospectrum and scalar variance spectrum are derived in HITSG for $Pr \ll 1$ and $Pr \gg 1$, and four comparisons are performed to assess the relevance of the model when the Prandtl number strongly departs from unity: this part serves as a new and additional validation of the present anisotropic modelling. The new numerical results of the present study are gathered in section 4. Effects of both very large and very small Prandtl numbers on the time evolution of $< \theta^2 >$ and $< u_3\theta >$ are firstly investigated, similarly to what was performed in HIT [18]: results are compared with the theoretical predictions of (BGC). Afterwards, the normalized mixed correlation $\rho_{w\theta}$ is studied as a function of the Reynolds and Prandtl numbers, and compared to results obtained in DNS. Furthermore, the effects of varying the Prandtl number on the small scales return to isotropy of the scalar second-order moments are analyzed. These different features are finally discussed in the concluding section 5.

2. Anisotropic EDQNM modelling for homogeneous turbulence

In this section, the main elements of Briard, Gomez and Cambon [7] (BGC) are reported to introduce the modelling of the passive scalar field and its flux in homogeneous isotropic turbulence with a mean scalar gradient (HITSG): definitions and evolution equations are recalled. In this configuration, the velocity field is decaying in an isotropic fashion and the mean scalar gradient produces scalar fluctuations so that the scalar variance $< \theta^2 >$ increases with time, with exponents proposed and assessed in [7].

2.1. *Modelling of the passive scalar and cospectrum*

In this first part, the modelling of the passive scalar field is addressed. The three two-point second-order spectral correlations of interest for the present study are the following ones: the spectral Reynolds tensor $\hat{R}_{ij}$ - or velocity-velocity correlation -, the scalar-scalar correlation $\mathcal{E}^T$, and the scalar flux F_i, or mixed velocity-scalar correlation. Their respective definitions are then

$$\hat{R}_{ij}(\boldsymbol{k},t)\delta(\boldsymbol{k}-\boldsymbol{p}) =< \hat{u}_i^*(\boldsymbol{p},t)\hat{u}_j(\boldsymbol{k},t) >, \tag{1}$$

$$\mathcal{E}^T(\boldsymbol{k},t)\delta(\boldsymbol{k}-\boldsymbol{p}) =< \hat{\theta}^*(\boldsymbol{p},t)\hat{\theta}(\boldsymbol{k},t) >, \tag{2}$$

$$F_i(\boldsymbol{k},t)\delta(\boldsymbol{k}-\boldsymbol{p}) =< \hat{u}_i^*(\boldsymbol{p},t)\hat{\theta}(\boldsymbol{k},t) >, \tag{3}$$

where $\hat{()}$ denotes the Fourier transform, $\hat{u}_i$ and $\hat{\theta}$ are respectively the spectral fluctuating velocity and scalar fields, and $\boldsymbol{k}$ and $\boldsymbol{p}$ are wavevectors. The exact evolution equations of $\hat{R}_{ij}$, $\mathcal{E}^T$, and F_i are

$$\left(\frac{\partial}{\partial t} + 2\nu k^2\right)\hat{R}_{ij}(\boldsymbol{k},t) = T_{ij}^{\mathrm{NL}}(\boldsymbol{k},t), \tag{4}$$

$$\left(\frac{\partial}{\partial t} + 2ak^2\right)\mathcal{E}^T(\boldsymbol{k},t) = T^{\mathrm{T,NL}}(\boldsymbol{k},t) - 2\lambda_j F_j(\boldsymbol{k},t), \tag{5}$$

$$\left(\frac{\partial}{\partial t} + (\nu+a)k^2\right)F_i(\boldsymbol{k},t) = T_i^{\mathrm{F,NL}}(\boldsymbol{k},t) - \lambda_j\hat{R}_{ij}(\boldsymbol{k},t), \tag{6}$$

where ν and a are the kinematic viscosity and the scalar diffusivity, $\lambda_j = \partial\Theta/\partial x_j$ is the mean scalar gradient along x_j, and T_{ij}^{NL}, $T^{\mathrm{T,NL}}$ and $T_i^{\mathrm{F,NL}}$ are respectively the kinetic, scalar, and scalar flux non-linear transfers.

In the HITSG framework, without mean-velocity gradients and helicity, the spectral Reynolds tensor is isotropic and simply reads

$$\hat{R}_{ij}(\boldsymbol{k},t) = \mathcal{E}_0(\boldsymbol{k},t)P_{ij}(\boldsymbol{k}), \qquad \mathcal{E}_0(\boldsymbol{k},t) = \frac{1}{2}\hat{R}_{ii}(\boldsymbol{k},t), \tag{7}$$

where $P_{ij} = (\delta_{ij} - \alpha_i\alpha_j)$, $\alpha_j = k_j/k$, and $\mathcal{E}_0$ is the isotropic kinetic energy density. The spherical average on a sphere S_k of radius k of these two-point correlations, which depend on the wavevector $\boldsymbol{k}$, yields the classical spectra that only depend on the wavenumber k. In particular, one obtains the kinetic energy spectrum E, the scalar variance spectrum E_T, and the cospectrum $\mathcal{F}$, according to

$$E(k,t) = \int_{S_k}\mathcal{E}_0(\boldsymbol{k},t)\mathrm{d}^2\boldsymbol{k}, \qquad E_T(k,t) = \int_{S_k}\mathcal{E}^T(\boldsymbol{k},t)\mathrm{d}^2\boldsymbol{k}, \tag{8}$$

$$\mathcal{F}(k,t) = \int_{S_k}F_3(\boldsymbol{k},t)\mathrm{d}^2\boldsymbol{k}. \tag{9}$$

From these spectra, one can define the one-point statistics, or integrated quantities, such as the kinetic energy $K(t)$, the scalar variance $K_T(t)$, the mixed velocity-scalar correlation $K_{\mathcal{F}}(t)$, and their respective dissipation rates $\epsilon(t)$, $\epsilon_T(t)$ and $\epsilon_{\mathcal{F}}(t)$:

$$K(t) = \frac{1}{2} < u_iu_i > = \int_0^\infty E(k,t)\mathrm{d}k, \qquad \epsilon(t) = 2\nu\int_0^\infty k^2E(k,t)\mathrm{d}k, \tag{10}$$

$$K_T(t) = < \theta^2 > = \int_0^\infty E_T(k,t)\mathrm{d}k, \qquad \epsilon_T(t) = 2a\int_0^\infty k^2E_T(k,t)\mathrm{d}k, \tag{11}$$

$$K_{\mathcal{F}}(t) = < u_3\theta > = \int_0^\infty \mathcal{F}(k,t)\mathrm{d}k, \qquad \epsilon_{\mathcal{F}}(t) = (\nu+a)\int_0^\infty k^2\mathcal{F}(k,t)\mathrm{d}k. \tag{12}$$

The departure from isotropy at the level of the scalar field is measured thanks to the deviatoric and symmetric tensor $H_{ij}^{(T)}$ defined as

$$2E_T(k,t)H_{ij}^{(T)}(k,t) = \int_{S_k}\left(\mathcal{E}^T(\boldsymbol{k},t) - \frac{E_T(k,t)}{4\pi k^2}\right)P_{ij}(\boldsymbol{k})\mathrm{d}^2\boldsymbol{k}. \tag{13}$$

Notably, $H_{ij}^{(T)}$ reflects directional anisotropy at the level of the scalar field, *i.e.* the

difference between the energy contained along $\boldsymbol{k}$ and the average energy. Since $\hat{\theta}$ is a scalar field, there is no polarization anisotropy (anisotropy between components). This decomposition comes from an expansion of $\mathcal{E}^T$ in spherical harmonics truncated at the first non-trivial order (the second one) as detailed in [7], and consistent with the expansion of the energy density $\mathcal{E}$ used for shear-driven flows [20, 21]. It is worth noting that such a decomposition is exact in HITSG [9].

Finally, the decomposition of the scalar flux reads

$$F_i(\boldsymbol{k},t) = \frac{3}{2}\mathcal{E}_j^F(k,t)P_{ij}(\boldsymbol{k}), \tag{14}$$

as detailed in (BGC): the vector $\mathcal{E}_j^F$ is real. For the axisymmetric configuration considered here in HITSG, only its third component along the mean scalar gradient is non-zero, so that $\mathcal{E}_3^F = \mathcal{F}/(4\pi k^2)$. Analogous expressions can be found for instance in [9, 12].

In the next part, the final evolution equations, arising from the present anisotropic EDQNM modelling for the passive scalar and its flux in HITSG, are given. A classical EDQNM procedure, as detailed in [7, 18] is used to close the non-linear transfers of the exact evolution equations (4), (5), and (6), and the previous decompositions for the two-point correlations are used to model anisotropy (at the scalar level) in both the non-linear and linear transfers.

2.2. *Final evolution equations and numerical setup*

In this section, a classical EDQNM procedure is used to close the non-linear transfers T_{ij}^{NL}, $T^{\mathrm{T,NL}}$ and $T_i^{\mathrm{F,NL}}$: all the details are given in (BGC) and the same constants for the kinetic and scalar eddy-damping terms are used here for consistency. In the end, the dynamics of HITSG is given by only four independent equations because of axisymmetry, which notably implies that $H_{11}^{(T)} = H_{22}^{(T)} = -H_{33}^{(T)}/2$:

$$\left(\frac{\partial}{\partial t} + 2\nu k^2\right) E(k,t) = S^{\mathrm{NL(iso)}}(k,t), \tag{15}$$

$$\left(\frac{\partial}{\partial t} + 2ak^2\right) E_T(k,t) = S^{\mathrm{T,NL(iso)}}(k,t) + 2\Lambda\mathcal{F}(k,t), \tag{16}$$

$$\left(\frac{\partial}{\partial t} + 2ak^2\right) E_T(k,t)H_{33}^{(T)}(k,t) = S_{33}^{\mathrm{T,NL(dir)}}(k,t) + \frac{2}{15}\Lambda\mathcal{F}(k,t), \tag{17}$$

$$\left(\frac{\partial}{\partial t} + (a+\nu)k^2\right) \mathcal{F}(k,t) = S_3^{\mathrm{F,NL}}(k,t) + \frac{2}{3}\Lambda E(k,t). \tag{18}$$

The first rhs terms like S^{NL} are the spherically-averaged non-linear transfers. In particular, $S_{33}^{\mathrm{T,NL(dir)}}$ reflects the directional anisotropy for the passive scalar field. The second rhs terms are the linear production terms, where the mean scalar gradient intensity is $\Lambda = -\lambda_3$ to ensure that the cospectrum $\mathcal{F}$ is positive.

Integration over the whole wavenumber space of the previous spectral equations yields $\partial_t K = -\epsilon$ for the kinetic energy since the velocity field is isotropic. And for

the scalar variance and scalar flux, one has

$$\frac{\partial K_T}{\partial t} = 2\Lambda K_{\mathcal{F}}(t) - \epsilon_T(t), \tag{19}$$

$$\frac{\partial K_{\mathcal{F}}}{\partial t} = \frac{2}{3}\Lambda K(t) - \epsilon_{\mathcal{F}}(t) + \underbrace{< p\frac{\partial \theta}{\partial x_3} >}_{\Pi_{\mathcal{F}}}. \tag{20}$$

In the last rhs term of (20), p is the fluctuating pressure, and the scalar-pressure correlation can be obtained by integrating $S_3^{\mathrm{F,NL}}$ over the whole wavenumber space: this term $\Pi_{\mathcal{F}}$ leads the return to isotropy (*i.e.* destruction) of the scalar flux, as detailed in [7], and is analogous to the pressure-strain tensor for the velocity field in shear flows for instance [21]. The pressure-scalar correlation is briefly addressed in section 4. Finally, the evolution equations of both ϵ_T and $\epsilon_{\mathcal{F}}$ are derived in Appendix A: these equations are not often considered and developed, and the authors believe it could be of interest to recall them.

In this work, two types of large scales initial conditions are addressed: Saffman and Batchelor turbulence, which correspond respectively to infrared slopes $\sigma = 2$ and $\sigma = 4$, where $E(k < k_L) \sim k^\sigma$, with k_L the integral wavenumber. This choice can be justified as follows. It has been shown recently that, despite the strong scatter of the decay exponents of the kinetic energy and scalar variance obtained in DNS and experiments, the values are mainly gathered between the theoretical predictions for Saffman and Batchelor turbulence [18, 22]. This is because the decay exponents mainly depend on the slope of the spectrum at the wavenumbers crossed by the integral scale during the decay, as shown in [23]. Since Saffman and Batchelor spectra cover most of the possible spectra, this makes these two configurations interesting, on top of their physical meaning, *i.e.* conservation of linear momentum for Saffman turbulence, and angular momentum for Batchelor turbulence. Furthermore, initial sharply peaked or Gaussian kinetic energy spectra would result in $E \sim k^4$ at large scales [24], which further justifies the relevancy of Batchelor turbulence.

Here, the initial conditions are isotropic, meaning that $\mathcal{F}(k, t = 0) = 0$, and are taken from [25]

$$E(k, t = 0) = K_0\, k^{-5/3}\, \epsilon^{2/3} f_L(kL)\, f_\eta(k\eta), \tag{21}$$

where f_L and f_η are shape functions for large and small scales respectively

$$f_L(x) = \left(\frac{x}{(x^{1.5} + 1.5 - \sigma/4)^{2/3}}\right)^{\frac{5}{3}+\sigma}, f_\eta(x) = \exp\Big(-5.3((x^4 + 0.4^4)^{\frac{1}{4}} - 0.4)\Big). \tag{22}$$

If not mentioned otherwise, we choose $E_T(k, t = 0) = E(k, t = 0)$ and a unit mean scalar gradient. Furthermore, it has been shown in (BGC) that without any loss of generality, one can always choose the same infrared slope for the kinetic energy and scalar spectra in HITSG.

The four previous generalized and spherically-averaged Lin equations for $\left(E, E_T, E_T H_{33}^{(T)}, \mathcal{F}\right)$ are solved using a third-order Runge-Kutta scheme with implicit treatment of diffusion terms. The wavenumber space is discretized using a logarithmic mesh $k_{i+1} = 10^{1/f} k_i$ where $f = 17$ is the number of points per decade. This mesh spans from $k_{\min}$ to $k_{\max}$, where $k_{\max}$ is either $10k_\eta$ for $Pr \leq 1$, or $10k_B$ for $Pr \geq 1$, where $k_\eta = (\epsilon/\nu^3)^{1/4}$ and $k_B = \sqrt{Pr}k_\eta$ are the Kolmogorov and Batch-

elor wavenumbers respectively. The time step is monitored by defining a constant CFL number and is obtained by considering the characteristic time scales of scalar and kinetic dynamics. The initial Reynolds number $Re_\lambda(0)$ is varied, roughly from $\sim 10^2$ to $\sim 10^5$: if not mentioned otherwise, the Reynolds number indicated when spectra are displayed is obtained after ten characteristic turnover times τ_0, where $\tau_0 = K(0)/\epsilon(0)$.

Finally, it is recalled that intermittency cannot be addressed with EDQNM: indeed, due to the physical hypothesis introduced to close the spectral evolution equations, EDQNM is rather suited for the investigation of second-order moments such as kinetic energy and scalar variance for instance, and third-order moments in HIT such as derivative skewnesses [26]. Therefore, higher-order moments, which could be strongly affected by intermittency, cannot be analyzed with EDQNM [1, 9].

Effects of a Prandtl number very different from unity on the dynamics of the cospectrum $\mathcal{F}(k,t)$ and of the scalar variance spectrum $E_T(k,t)$ are investigated in section 3. Notably, the scaling in the inertial range of the spectral velocity-scalar correlation is addressed, and comparisons with recent numerical works are performed in order to assess the present anisotropic EDQNM modelling in configurations different from the ones proposed in [7] where $Pr = 1$.

3. Inertial scaling of $E_T(k,t)$ and $\mathcal{F}(k,t)$ for $Pr \neq 1$ - Comparisons

The emphasis is put on the inertial scaling of the scalar variance spectrum $E_T(k,t)$ and cospectrum $\mathcal{F}(k,t)$ when the Prandtl number is either very low or very large. These theoretical scalings are recovered analytically and numerically, and are then compared with recent numerical studies, such as DNS, LES and other spectral models. The fact that the present results are not always compared with DNS is because in most of the DNS, either the Reynolds number is not high enough, or the Prandtl number is too close to unity.

The successful comparisons proposed here notably illustrate that the anisotropic EDQNM modelling developed in [7] can be applied as well for highly and weakly diffusive passive scalar fields.

3.1. *Highly diffusive passive scalar: $Pr \ll 1$*

It is recalled that for $Pr \ll 1$, after the classical inertial-convective range where $E_T \sim \epsilon_T \epsilon^{-1/3} k^{-5/3}$, the inertial-diffusive range spans from the Corrsin-Obukhov wavenumber $k_{CO} = Pr^{3/4} k_\eta$, where diffusion effects become dominant [27], to the Kolmogorov wavenumber k_η. In the framework of completely homogeneous isotropic turbulence, without any mean scalar gradient, the authors defined a convective-diffusive wavenumber $k_{CD} = \sqrt{Pr}\, k_\eta$ from which small scales convection balances diffusion [28]. In this section, both the inertial scalings of E_T and $\mathcal{F}$ are investigated and assessed numerically.

In HIT, the scalar spectrum scales in the inertial-diffusive range as [27]

$$E_T(k,t) = \frac{K_0}{3}\, \epsilon_T\, a^{-3}\, \epsilon^{2/3}\, k^{-17/3}, \tag{23}$$

where $K_0 \simeq 1.4$ is the Kolmogorov constant. Such a scaling was notably recovered with EDQNM numerous times [18, 28, 29]. It has been shown that with an additional mean scalar gradient Λ sustaining the scalar fluctuations, the scalar dissipation rate ϵ_T should take into account this production mechanism [30], thus

leading to

$$\underbrace{\epsilon_T}_{\text{HIT}} \rightarrow \underbrace{\epsilon_T + 2a\Lambda^2}_{\text{HITSG}}, \tag{24}$$

where $2a\Lambda^2$ is a pseudo scalar dissipation rate arising because of the presence of the mean gradient. The HIT scaling for E_T given in (23) is thus modified in HITSG into

$$E_T(k,t) = \frac{K_0}{3}\,\epsilon_T\,a^{-3}\,\epsilon^{2/3}\,k^{-17/3}\left(1 + 2\frac{a\Lambda^2}{\epsilon_T}\right). \tag{25}$$

Such a result was recovered analytically with the Sparse Direct-Interaction Perturbation (SDIP) [15]. Here, an alternative method is proposed, based on dimensional analysis and physical arguments that are consistent with further developments. In the HITSG framework, the integration of the scalar Lin equation (16) directly yields

$$\frac{\partial K_T}{\partial t} = -\epsilon_T\left(1 + \frac{2\Lambda K_{\mathcal{F}}}{\epsilon_T}\right). \tag{26}$$

The whole rhs term can be seen as a general scalar dissipation rate, and dimensional analysis gives $K_{\mathcal{F}} \sim \Lambda a$ which results into (24).

The present simulations, at very low Prandtl numbers and very large Reynolds numbers, show that $2a\Lambda^2/\epsilon_T \ll 1$, so that the classical scaling (23) is still relevant. This is consistent with the return to isotropy of small scales in the inertial-diffusive range at large Reynolds numbers: this feature will be illustrated in section 4.3. However, when a moderate Reynolds number is combined with a very small Pr, this ratio becomes greater than unity, so that the isotropic scaling is modify into

$$E_T(k,t) \sim \Lambda^2\,a^{-2}\,\epsilon^{2/3}\,k^{-17/3}, \tag{27}$$

derived in [16, 17], and is notably obtained by neglecting the non-linear contribution in the scalar Lin equation with respect to production and dissipation. It is worth noting that in [17], the Prandtl number is very low, and the Reynolds number moderate, so that very likely small scales are still anisotropic due to production mechanisms. Consequently, the general expression (25) should be kept, since it gives, for the inertial-diffusive scaling, both the isotropic expression and the anisotropic correction, for large and moderate Reynolds numbers respectively.

The $k^{-17/3}$ scaling of the scalar spectrum for low Prandtl numbers in HITSG has been assessed recently by DNS [17]. Present results are compared with the latter DNS in figure 1(a). The final Reynolds number is $Re_\lambda = 240$ after ten turnover times. The Prandtl number is $Pr = 1/2048$, and initially the integral scales are $L(0) = 1.346$ and $L_T(0) = 3.468$, and $E_T(k, t = 0) = 0$, so that the scalar fluctuations arise from the mean scalar gradient. A good agreement is found for the scalar spectrum $k^{-17/3}$ scaling in the inertial-diffusive range. Near the Kolmogorov wavenumber ($k\eta = 1$), our scalar spectrum slightly increases, and this is probably due to small scale convection [28]: the latter phenomenon increases with higher Reynolds numbers and lower Prandtl numbers. This does not happen in the DNS result, very likely because small scales are not completely resolved beyond k_η: indeed $k_{\max} = 1.347k_\eta$ in the DNS, whereas $k_{\max} = 10k_\eta$ here. Nevertheless, the $k^{-17/3}$ is well recovered over two decades, which is the most important feature.

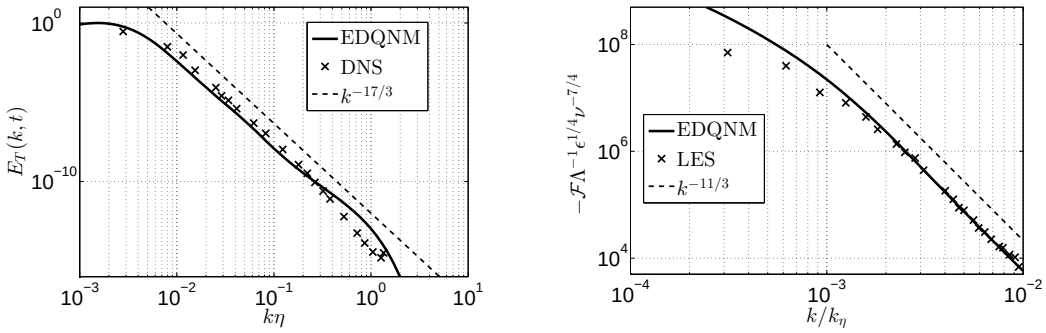

(a) (b)

Figure 1. (a) Scalar spectrum scaling $E_T(k,t) \sim k^{-17/3}$ obtained with EDQNM compared to DNS [17], with $Pr = 1/2048$ and $\sigma = 2$ at $Re_\lambda = 240$. (b) Cospectrum scaling $\mathcal{F} \sim k^{-11/3}$ obtained with EDQNM compared with the LES [15], with $Pr = 2.10^{-4}$, $Re_\lambda = 1500$, and $\sigma = 2$.

We now move on with the determination of the cospectrum inertial scaling. The starting point is the cospectrum Lin equation (18). A reasonable hypothesis when the Prandtl number is very low is to assume that the diffusive timescale $(ak^2)^{-1}$ is much smaller than the non-linear one

$$\tau(k) = \Big(k^3 E(k)\Big)^{-1/2} = \Big(k^2\epsilon\Big)^{-1/3} = \frac{kE(k)}{\epsilon}. \tag{28}$$

This is obvious at large k for high thermal diffusivity a. Therefore, non-linear contributions can be neglected, consistently with the argument for the scaling (27). Then, for scaling considerations, the time derivative is dropped off, so that

$$ak^2\mathcal{F}(k,t) = \frac{2}{3}\Lambda E(k,t), \tag{29}$$

which yields the inertial-diffusive range scaling for the cospectrum

$$\mathcal{F}(k,t) = \frac{2}{3}K_0\Lambda a^{-1}\epsilon^{2/3}k^{-11/3}. \tag{30}$$

A similar process was performed in [15, 16, 17], the key point being to neglect the non-linear transfers. Another approach is possible: it was shown numerically in [7] at $Pr = 1$, consistently with DNS and experiments, that the normalized cospectrum correlation

$$\rho_{w\theta} = \frac{< u_3\theta >}{\sqrt{< u_3^2 >< \theta^2 >}}, \tag{31}$$

where $u_3 = w$, is constant at large Reynolds numbers. One can define an analogous spectral normalized cospectrum as constant in the inertial range [17]. Hence, using Kolmogorov scaling for E, and scaling (23) for E_T, one gets

$$\rho_{w\theta}(k) = \frac{\mathcal{F}(k)}{\sqrt{E(k)E_T(k)}} \Leftrightarrow \mathcal{F}(k,t) \sim a^{-3/2}\epsilon_T^{1/2}\epsilon^{2/3}k^{-11/3}. \tag{32}$$

Moreover, since the scalar field as no retro-action on the velocity one, ϵ_T should not appear in (32): one can recover (30) by replacing ϵ_T with $a\Lambda^2$, as already done previously.

The $k^{-11/3}$ inertial-diffusive scaling of the cospectrum for $Pr \ll 1$ is assessed in figure 1(b): our EDQNM simulation with $E_T(k, t = 0) = 0$ is compared to the LES [15] where $Pr = 2.10^{-4}$ and $Re_\lambda = 1500$ (after 10 turn-over times for EDQNM). The agreement with the $k^{-11/3}$ is rather good at this Reynolds number, and the agreement between EDQNM and LES is excellent in the inertial-diffusive range.

3.2. *Weakly diffusive passive scalar: Pr* $\gg 1$

The case $Pr \gg 1$ is now considered: small scales of the scalar variance spectrum experience convection from the velocity field of the Kolmogorov scale, which results in a viscous-convective range from k_η, the smallest active turbulent scale for the velocity field, to the Batchelor wavenumber $k_B = \sqrt{Pr} k_\eta$, where E_T scales as [31]

$$E_T(k, t) = K_B \epsilon_T \sqrt{\frac{\nu}{\epsilon}} k^{-1}, \tag{33}$$

where K_B is the Batchelor constant, found to be $\simeq 2.5$ in the present simulations. This value is close to the first proposal by Batchelor [31] $K_B = 2$, and in agreement with Gibson's predictions [32] $\sqrt{3} \leq K_B \leq 2\sqrt{3}$ for HIT. Other values measured in the ocean are slightly higher (see [33] and values reported therein) even though other mechanisms may play a non-negligible role in this environment. Values obtained in DNS at moderate Re_λ are also slightly higher [34, 35].

Then, beyond k_B, scalar fluctuations are destroyed by diffusive processes. Interactions that are at the origin of the viscous-convective range are strongly non-local. As already done numerous times, non-local expansions from very large to very small scales are added to the scalar (isotropic) non-linear transfers of equation (16): theoretical details are gathered in [19], and some applications within the EDQNM framework were thoroughly examined recently [18, 26].

The scaling of the cospectrum $\mathcal{F}(k, t)$ for a weakly diffusive passive scalar field has been discussed notably in [15] and it has been found that the spectral velocity-scalar correlation is not strongly modified in the framework $Pr \gg 1$, unlike the case $Pr \ll 1$. This is expected if one compares the cospectrum Lin equations (18) for $Pr = 1$ where $a = \nu$, so that the dissipative term is $2\nu k^2 \mathcal{F}$, and for $Pr \gg 1$, where $a \ll \nu$, which yields for the dissipative term only $\nu k^2 \mathcal{F}$. Hence, for a weakly diffusive scalar, the cospectrum still scales in $k^{-7/3}$ in the inertial-convective range.

Finally, two comparisons are proposed hereafter. Since in DNS when the Prandtl number increases, the Reynolds number conjointly decreases for numerical resolution issues, we first propose a large Reynolds number comparison with the SDIP model [15] at $Pr = 100$ in figure 2(a). However, since the SDIP model provides asymptotically large Reynolds numbers results, the Reynolds number is unknown. The agreement is acceptable, and the slight discrepancy may be attributed to the uncertainty for the Reynolds numbers, which is $Re_\lambda = 2.10^4$ here with the present anisotropic EDQNM modelling.

Then, in figure 2(b), the compensated scalar variance spectrum is compared with the low Reynolds number DNS of Yeung and coworkers [36], where $Re_\lambda \simeq 8$ and $Pr = 1024$. Initially, the scalar variance spectrum is zero, and the Reynolds number is chosen so that after ten turnover times the Reynolds number is $Re_\lambda = 10$. Our minimum wavenumber was decreased on purpose to match with the DNS configuration, and the reason for the slight discrepancy at large wavenumbers could be that the DNS is forced at large scales, whereas here we have a freely decaying Saffman turbulence. This does not prevent us from getting a very good agreement, both in the viscous convective range and further in the viscous-dissipative range,

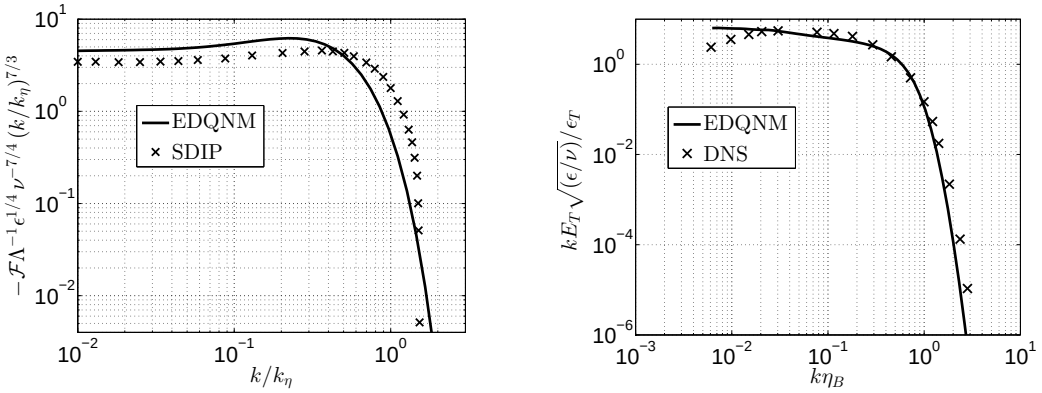

(a) (b)

Figure 2. (a) Compensated cospectrum compared with the SDIP model [15] at $Re_\lambda = 2.10^4$ and $Pr = 100$. (b) Compensated scalar variance spectrum compared with the DNS [36] at $Re_\lambda \simeq 8$ and $Pr = 1024$.

which validates our approach, even at low Reynolds numbers.

3.3. *Spectral transfers and conclusions for the inertial scalings*

The inertial scalings of the cospectrum $\mathcal{F}(k,t)$ and scalar variance spectrum $E_T(k,t)$ were investigated for both low and large Prandtl numbers in subsections 3.1 and 3.2, where a mean scalar gradient Λ sustains the fluctuations in a homogeneous isotropic decaying turbulence. The theoretical predictions were recovered analytically, and more importantly, assessed numerically over a wide range of Reynolds and Prandtl numbers, which illustrates the relevance of our anisotropic EDQNM modelling.

- For a highly diffusive scalar, E_T and $\mathcal{F}$ scale respectively in $k^{-5/3}$ and $k^{-7/3}$ in the inertial-convective range, and then, from the Corrsin-Obukhov wavenumber k_{CO}, in $k^{-17/3}$ and $k^{-11/3}$ in the inertial-diffusive range. For illustration purposes, these spectra are displayed in figure 3(a) for Saffman turbulence at very large Re_λ and $Pr = 10^{-5}$. The less steep slope while approaching k_η is due to small scales convection and this was addressed in [28]: here, the emphasis is put on the spectral scalings $k^{-17/3}$ and $k^{-11/3}$ which are recovered numerically with the present anisotropic EDQNM modelling at large Reynolds numbers, and with a clear separation of dominant mechanisms at k_{CO} between large scales convection and diffusion.
- For a weakly diffusive scalar, the viscous-convective range in k^{-1} from k_η to k_B is not modified by the presence of a mean scalar gradient for $E_T(k,t)$: this is illustrated in figure 3(b). Furthermore, there is no viscous-convective range for the cospectrum: instead, $\mathcal{F}$ decays slightly later, in terms of wavenumbers, when $Pr = 10^4$ than with $Pr = 1$, because the viscous dissipation is reduced, as explained earlier.

Finally, the budget terms of the evolution equation of $E_T(k,t)$ are analyzed in figure 4, for large (left column) and low (right column) Reynolds numbers, at high (top line) and small (bottom line) Prandtl numbers. The first observation is that for all four cases, the linear production term is more intense than the non-linear transfer at large scales, and then is negligible at smaller scales, meaning that production of scalar fluctuations through the mean gradient is dominant at large scales: it will be illustrated in section 4.3 that anisotropy is consistently gathered

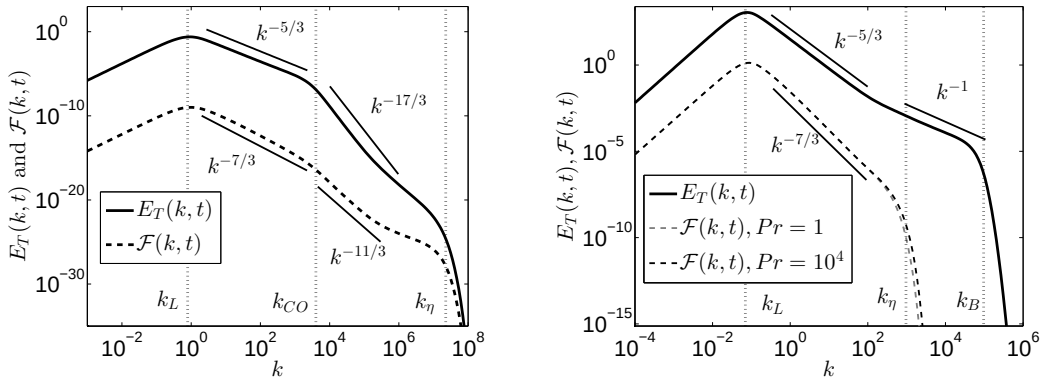

Figure 3. Scalar variance spectrum $E_T(k,t)$ and cospectrum $\mathcal{F}(k,t)$ at large Reynolds numbers for $\sigma = 2$. (a) $Re_\lambda = 2.10^5$ and $Pr = 10^{-5}$, along with the integral, Corrsin-Obukhov and Kolmogorov wavenumbers k_L, k_{CO} and k_η. (b) $Re_\lambda = 10^4$ and $Pr = 10^4$, along with the integral, Kolmogorov and Batchelor wavenumbers k_L, k_η and k_B. The cospectrum at $Pr = 1$ at the same Reynolds numbers is displayed in grey as well.

at these scales.

In the very large Péclet number case (a) where $Pe_\lambda = Re_\lambda\sqrt{Pr} = 1.8\,10^5$, there is a clear separation of three domains, in agreement with [17], even though freely decaying turbulence is considered here: at low wavenumbers, one has almost $-S^{\mathrm{T,NL(iso)}} \simeq 2\Lambda\mathcal{F}$, and the difference is due to the term $\partial_t E_T \neq 0$; at intermediate wavenumbers, all three contributions are very small and of the same order; finally, at large wavenumbers, there is a balance between non-linear transfer and dissipation $S^{\mathrm{T,NL(iso)}} \simeq 2ak^2 E_T$.

In the opposite case (d) where $Pe_\lambda \to 0$, non-linear transfers are small and production balances well dissipation, in agreement with the prediction of [17]. Furthermore, in the two low Prandtl number cases (c) and (d), the insets show that the dissipation term is always more intense that non-linear transfers, even in the high Re_λ configuration, in accord with the latter reference. For the two high Prandtl number cases (a) and (b), non-linear transfers are more intense around k_η, and then dissipation takes over while approaching k_B at larger wavenumbers.

4. Time evolution and anisotropy

In section 3, the present anisotropic EDQNM modelling was assessed for small and large Prandtl numbers in HITSG, for both low and high Reynolds numbers, by investigating the inertial scalings of the scalar variance spectrum $E_T(k,t)$ and cospectrum $\mathcal{F}(k,t)$. In this part, effects of the Prandtl number Pr on the time evolution of the scalar variance K_T, the mixed-correlation $K_\mathcal{F}$, the normalized cospectrum correlation $\rho_{w\theta}$, and the Nusselt number Nu, are analyzed, along with the small scales return to isotropy of the flow. Effects of Prandtl numbers at moderate Reynolds numbers are discussed as well.

4.1. *Prandtl effects on the decay and growth of $< u_3\theta >$ and $< \theta^2 >$*

The growth of $K_T =< \theta^2 >$ and decay of $K_\mathcal{F} =< u_3\theta >$ are addressed for both highly and weakly diffusive passive scalars. This part is a direct application of the modelling developed in [7] and of the theoretical exponents derived therein and

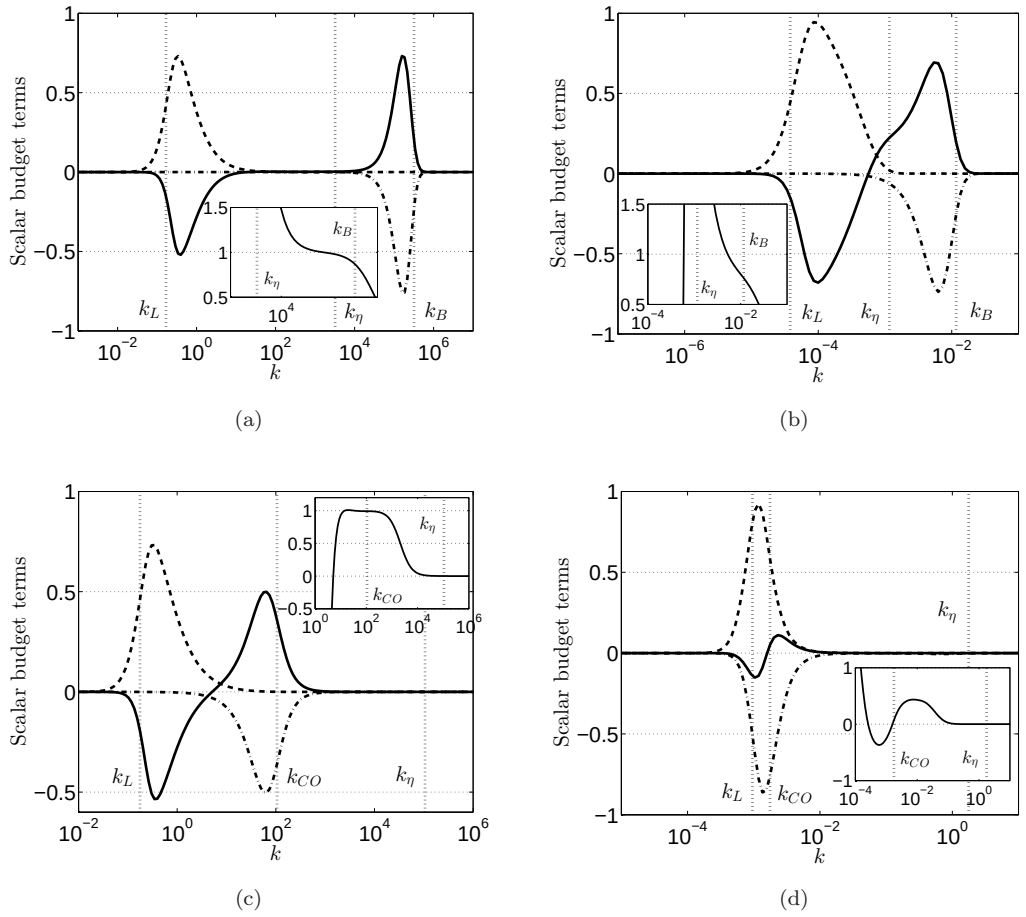

Figure 4. Budget terms of the evolution equation (16) of the scalar variance spectrum $E_T(k,t)$, along with the previous characteristic wavenumbers, for $\sigma = 2$. − Non-linear term $kS^{\mathrm{T,NL(iso)}}$; −− Production term $2k\Lambda\mathcal{F}$; −· Dissipation term $-2ak^3E_T$. The insets represent the ratio $S^{\mathrm{T,NL(iso)}}/2ak^2E_T$. (a) $Re_\lambda = 1800$ and $Pr = 10^4$, (b) $Re_\lambda = 23$ and $Pr = 10^2$, (c) $Re_\lambda = 2.10^4$ and $Pr = 10^{-4}$, and (d)$Re_\lambda = 400$ and $Pr = 10^{-4}$.

recalled here:

$$K_{\mathcal{F}}(t) \sim t^{\alpha_{\mathcal{F}}}, \qquad \alpha_{\mathcal{F}} = -\frac{\sigma - p_{\mathcal{F}} - 1}{\sigma - p_E + 3}, \tag{34}$$

$$K_T(t) \sim t^{\alpha_T^\Lambda}, \qquad \alpha_T^\Lambda = \frac{1}{2}\frac{p_{\mathcal{F}} - p_E + 8}{\sigma - p_E + 3}, \tag{35}$$

where σ is the infrared slope of the kinetic energy spectrum, *i.e.* $E(k < k_L) \sim k^\sigma$, p_E and $p_{\mathcal{F}}$ are the kinetic and cospectrum backscatter parameters: in Batchelor isotropic turbulence $p_E \simeq 0.55$, whereas it is zero for $\sigma \leq 3$ [19, 24, 37].

In [7] for $Pr = 1$, one had $p_{\mathcal{F}} = 0.4075$. Here, for $Pr \ll 1$ and $Pr \gg 1$, it is found that $p_{\mathcal{F}}$ slightly increases to $p_{\mathcal{F}} \simeq 0.42$ when Pr departs from unity, consistently with the variations of the scalar backscatter parameter p_T in HIT with Pr [18]. It makes sense that $p_{\mathcal{F}}$ varies less with Pr than p_T since $< u_3\theta >$ is a mixed correlation where the velocity field is not affected at all by a change in Pr.

The theoretical decay exponent of the kinetic energy is also recalled [18, 19, 22]

$$K(t) \sim t^{\alpha}, \qquad \alpha = -2\frac{\sigma - p_E + 1}{\sigma - p_E + 3}, \tag{36}$$

where for Saffman and Batchelor turbulence, one has respectively $K \sim t^{-6/5}$ and $K \sim t^{-1.38}$.

In figures 5(a) and 5(b), both theoretical predictions for $\alpha_{\mathcal{F}}$ and α_T^{Λ} given in (34) and (35) are recovered numerically. The Reynolds number Re_λ is much higher for $Pr \ll 1$ than for $Pr \gg 1$ in order to keep a sufficiently high Péclet number. One can say from figures 5(a) and 5(b) that the respective decay and growth of $K_{\mathcal{F}}$ and K_T in HITSG is not affected by high or small Prandtl numbers at large Reynolds numbers. A similar result was obtained for scalar integrated quantities such as K_T in decaying HIT [18].

In addition, α_T^{Λ} is presented in figure 5(c) at moderate Reynolds numbers, typical of DNS and experiments, for various Prandtl numbers. This figure should be compared to the case $Pr = 1$ presented in [7] and recalled in grey in figure 5(c), where a monotonic decrease of α_T^{Λ} is observed from the high Reynolds to the low Reynolds predictions. Therefore, this figure clearly illustrates that even though a Pr strongly different from unity does not modify the asymptotic theoretical predictions at very large Reynolds numbers, it significantly alters the decay of the scalar variance K_T at moderate ones. For $Pr \gg 1$, the growth exponent α_T^{Λ} slightly increases before diminishing toward the low Reynolds numbers ($Re_\lambda \leq 1$) predictions of [7]: this is because when Re_λ decreases, the $k^{-5/3}$ inertial range vanishes. However, the k^{-1} viscous range survives temporarily, thus slightly slowing down the decay. Whereas for $Pr \ll 1$, the decrease of α_T^{Λ} starts at quite high Reynolds numbers, because the Péclet number is very small. The same observations are made for the decay exponent $\alpha_{\mathcal{F}}$ of the mixed-correlation.

Consequently, one could conclude from figure 5(a), 5(b) and 5(c) that the Prandtl number does not affect the time exponent at very large Reynolds numbers, but at moderate ones. This is of importance because it could explain why in DNS there is a significant scatter of the normalized mixed-correlation $\rho_{w\theta}$ for instance, addressed in the next part.

As a direct application of the theoretical decay exponents, the scalar-pressure correlation $\Pi_{\mathcal{F}} =< p\partial_3\theta >$ is investigated: this correlation has not received much attention, even though it is the destruction mechanism of the scalar flux. In [7], it was shown that one cannot define a decay rate for the dissipation $\epsilon_{\mathcal{F}}$ at large Reynolds numbers, because it is not conserved in the inertial range unlike ϵ and ϵ_T. But it is possible for $\Pi_{\mathcal{F}}$: indeed, according to the evolution equation (20) of $< u_3\theta >$, $\Pi_{\mathcal{F}}$ should evolve in time similarly to the production mechanism, which is proportional to the kinetic energy $K(t)$. This is confirmed numerically in figure 6 for Saffman turbulence: $\Pi_{\mathcal{F}}$ is found to decay in $t^{-6/5}$, as the kinetic energy. Furthermore, figure 6 once more illustrates that the theoretical decay rate does not depend on the Prandtl number.

4.2. *Normalized cospectrum correlation $\rho_{w\theta}$ and Nusselt number Nu*

The normalized correlation $\rho_{w\theta}$, defined in (31), is addressed in figure 7(a). Some values of this quantity at $Pr = 1$ were reported in [7]: therefore, the emphasis is put here on the influence of Pr on $\rho_{w\theta}$. The first feature to point out is that at large Reynolds numbers, either with a small or large Prandtl number, $\rho_{w\theta}$ is constant: this can be obtained analytically by considering the exponents (34)-(36). Then, $\rho_{w\theta}$ diminishes with decreasing Reynolds numbers because of the joint decay of $< u_3\theta >$ and growth of the scalar variance, both studied in the previous part. It is worth noting that the magnitude of $\rho_{w\theta}$ strongly depends on Pr at moderate Re_λ, because the Prandtl number affects decay exponents in this region of moderate Reynolds numbers, as revealed previously in figure 5(c).

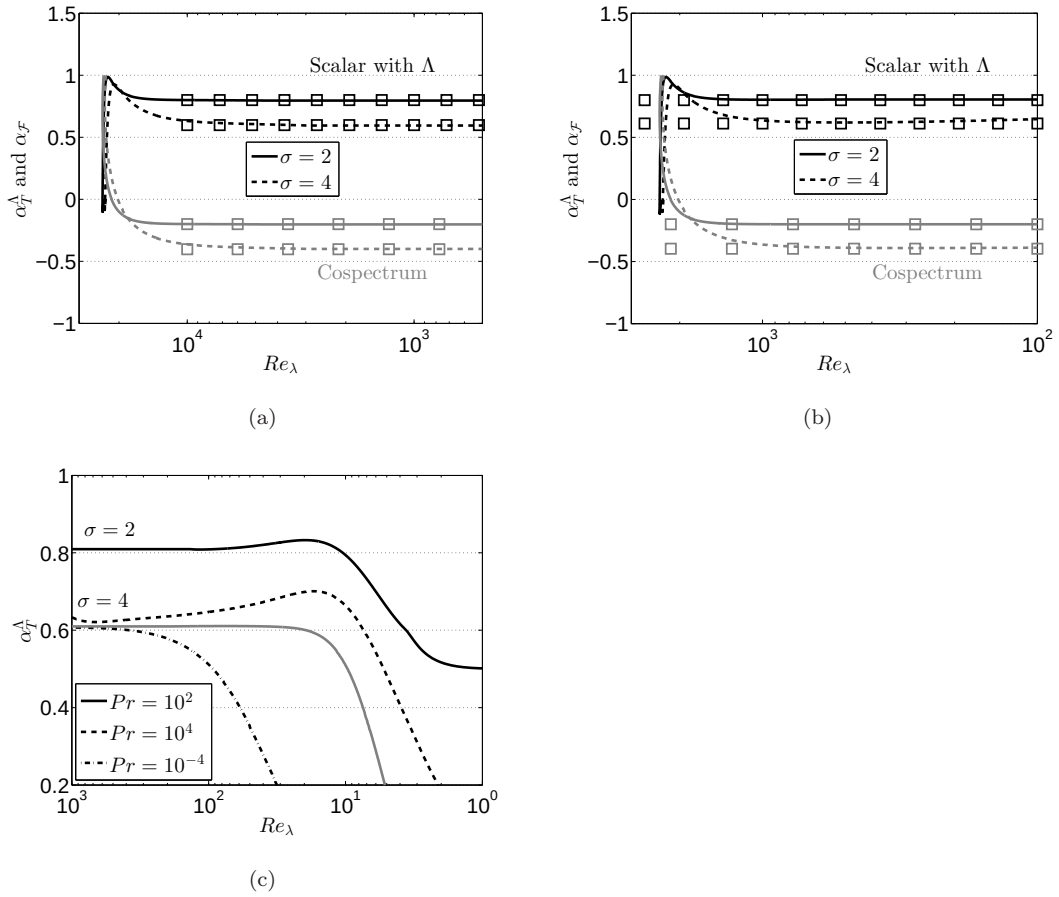

Figure 5. Scalar growth exponent α_T^Λ defined in (35) (black lines), and cospectrum decay exponent $\alpha_\mathcal{F}$ defined in (34) (grey lines). Simulations $\sigma = 2$ (-) and $\sigma = 4$ (- -), with □ the theoretical predictions, for (a) $Pr = 10^{-4}$ and (b) $Pr = 10^4$. (c) α_T^Λ at intermediate Reynolds numbers, for both $\sigma = 2$ and $\sigma = 4$ and various Pr (in black); the case $\sigma = 4$ and $Pr = 1$ is recalled in grey.

In addition, several low Pr values from the DNS [17] are included in figure 7(a), and there is a good quantitative agreement with the present anisotropic EDQNM modelling: the three simulations of [17], for $Pr = 1/2048$, $Pr = 1/512$, and $Pr = 1/128$, are almost all consistently contained within our EDQNM simulations at $Pr = 10^{-4}$ and $Pr = 10^{-2}$. Moreover, at these moderate Re_λ, it is recovered that $\rho_{w\theta}$ increases in magnitude with the Reynolds number at a given Prandtl number.

Furthermore, an interesting behaviour is recovered, which is the decrease in magnitude of $\rho_{w\theta}$ when Pr departs from unity, either for $Pr \ll 1$ or $Pr \gg 1$, at a fixed moderate Re_λ: this notably confirms the DNS results and predictions of [17, 35], and can be interpreted in terms of loss of phase alignment between spectral velocity and scalar fluctuations: indeed, for both $Pr \ll 1$ and $Pr \gg 1$, there exists a subrange in wavenumber space (the inertial-diffusive and viscous-convective ranges respectively) where the scalar variance spectrum strongly depart from the kinetic energy one. This phenomenon is much more visible for $Pr \ll 1$.

This decrease in magnitude of $\rho_{w\theta}$ with a Prandtl number different from unity is of practical interest since it happens at moderate Reynolds numbers only. This might be an additional reason for the scattering of the obtained values of the normalized correlation $\rho_{w\theta}$, in addition of moderate Reynolds numbers effects, already mentioned in [7].

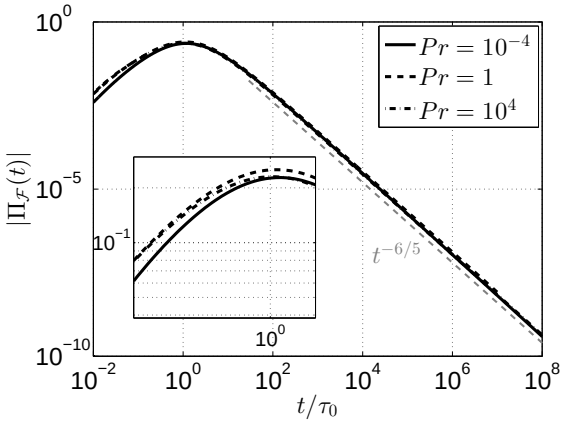

Figure 6. Pressure-scalar correlation $\Pi_{\mathcal{F}}$ for $\sigma = 2$ at various Prandtl numbers as a function of the normalized time, where τ_0 is the initial eddy turnover time. The grey dashed line corresponds to the theoretical prediction. The zoom focuses on small times to illustrate the small difference with varying Pr.

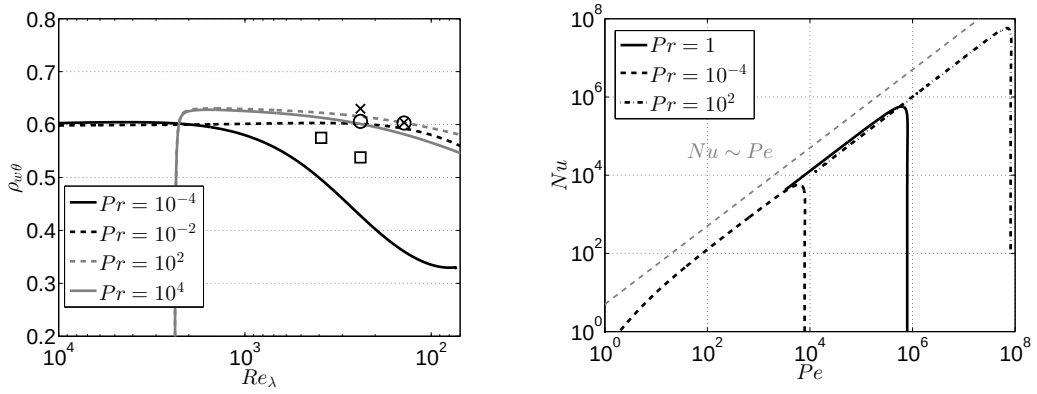

(a) (b)

Figure 7. (a) Normalized correlation $\rho_{w\theta}$ for Batchelor turbulence ($\sigma = 4$) at various Prandtl numbers as a function of Re_λ: results are very similar for Saffman turbulence. Symbols correspond to the DNS [17]: □ $Pr = 1/2048$; ◯ $Pr = 1/512$; × $Pr = 1/128$. Black and grey lines are respectively for small and large Prandtl numbers. (b) Nusselt number Nu, defined in (37), as a function of the Péclet number Pe, for various Pr.

Finally, the Nusselt number, defined as

$$Nu = -\frac{< u_3\theta >}{a\Lambda}, \tag{37}$$

is investigated for various Prandtl numbers. Nu is in fact another normalization of the mixed-correlation $< u_3\theta >$ which is of practical interest for heat transfers. The theoretical prediction for the Nusselt number, detailed and assessed in [38], is that it should vary as $Nu \sim Pe$, where the Péclet number is $Pe = PrRe_T$, with the turbulent Reynolds number $Re_T = 3Re_\lambda^2/20$. This scaling is successfully recovered in figure 7(b) for a wide range of Péclet and Prandtl numbers.

4.3. *Scale-by-scale distribution of anisotropy*

The anisotropy of the flow is investigated here, at the level of the scalar second-order moments: it is recalled that in [7], it was shown that small scales were completely returning to isotropy at $Pr = 1$ in HITSG, which is expected since the velocity field

remains isotropic. Consequently, one can wonder if the Prandtl number has an influence on the scalar small scales return to isotropy. It is important to precise here that with EDQNM, one cannot investigate third-order moments such as derivative skewnesses, except in HIT where there are expressions which link third-order moments and non-linear transfers [26].

The scale by scale analysis of anisotropy is done thanks to the symmetric and deviatoric tensor $H_{ij}^{(T)}(k,t)$, defined in (13), which measures directional anisotropy at the level of the scalar second-order moments: if $H_{ij}^{(T)}(k_1 < k < k_2) = 0$, it means that the scales between k_1 and k_2 are isotropic.

As expected, it is found hereafter that the impact of the Prandtl number on the return to isotropy of small scales is comparable for instance to moderate Reynolds numbers effects for the kinetic field in shear flows [21]: indeed, the relevant dimensionless parameter for the scalar is not only Re_λ, but the product $Re_\lambda\sqrt{Pr}$, which could be called a Taylor Péclet number Pe_λ.

Thus, even with a large Re_λ, if the Prandtl number is as small as 10^{-4}, Pe_λ will be moderately small, so that scalar small scales may not be not completely isotropic, in addition to other issues, such as the lack of scale separation in the spectra [17]. Consequently, very large Re_λ are required for highly diffusive passive scalars. This is illustrated in figure 8(a), where the Taylor Reynolds number is very large $Re_\lambda \sim 10^5$, so that even at small Prandtl numbers of order $\sim 10^{-4}$, the Péclet number based on the Taylor scale is still sufficiently high $Pe_\lambda \sim 10^3$: this is an important condition for weakly diffusive passive scalars to obtain clear scalings, as underlined in [17]. This allows to observe in figure 8(a) that there is a complete return to isotropy of scalar second-order moments small scales. It is worth noting that from the Corrsin-Obukhov wavenumber k_{CO}, *i.e.* in the inertial-diffusive range, there is no more anisotropy: the non-linearity being much stronger in the inertial-convective range, for $k_L < k < k_{CO}$, the return to isotropy mechanism occurs dominantly in this region of the wavenumber space.

For a weakly diffusive scalar field, analogous assessments leading to a similar conclusion are made in [35], where it is shown numerically that even with a moderate Re_λ, increasing the Pr - which amounts to increase Pe_λ - allows to recover scalar isotropic small scales. It is proposed to illustrate this feature in figure 8(b), where $H_{33}^{(T)}$ is displayed for Saffman turbulence at $Re_\lambda = 100$, for $Pr = 1$ and $Pr = 10^4$. It is clear, notably with the zoom around the Kolmogorov wavenumber k_η, that increasing the Prandtl number at a fixed Reynolds number participates into restoring isotropy at small scales.

It is recalled that a complete return to isotropy of scalar second-order moments at small scales is not incompatible with third-order moments being anisotropic at these same scales, as shown for HITSG in [6]. However, with a model based on a EDQNM closure, third-order moments such as derivative skewnesses are accessible only in HIT [26], so that they cannot be investigated here in HITSG.

Finally, within our modelling, according to figures 8(a) and 8(b), the large scales level of anisotropy seems to be independent of the Prandtl number in Saffman turbulence, and always very close to 1/15, with $1/15 \geq H_{33}^{(T)}$. This value of 1/15 is interesting because it is the maximum level of anisotropy that the scalar field can handle: indeed, the exact expansion for the spectral scalar-scalar correlation in HITSG reads [7]

$$\mathcal{E}^T(\boldsymbol{k},t) = \frac{E_T(k,t)}{4\pi k^2}\Big(1 - 15H_{pq}^{(T)}(k,t)\alpha_p\alpha_q\Big), \tag{38}$$

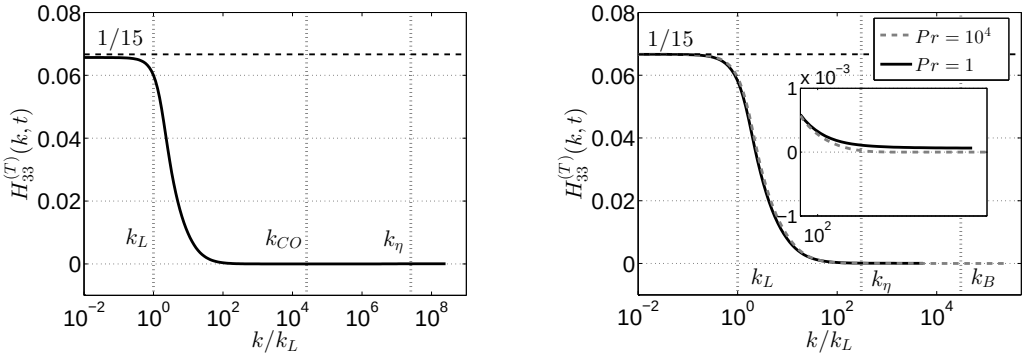

Figure 8. Prandtl number effect on the small scales return to isotropy using $H_{33}^{(T)}(k,t)$ in Saffman turbulence $\sigma = 2$. The integral and Kolmogorov wavenumbers k_L and k_η are indicated. The horizontal dashed line indicating 1/15 refers to the maximal level of anisotropy detailed in the text. (a) $Pr = 10^{-4}$ and $Re_\lambda = 2.10^5$ so that $Pe_\lambda = 2.10^3$. The Corrsin-Obukhov wavenumber $k_{CO} = k_\eta Pr^{3/4}$ is displayed. (b) $Pr = 1$ in black and $Pr = 10^4$ in grey, both at $Re_\lambda = 100$, so that the Péclet number varies from $Pe_\lambda = 10^2$ to 10^4. The Batchelor wavenumber $k_B = k_\eta\sqrt{Pr}$ is displayed.

and a realizability condition was thus derived in BGC, namely

$$\max\left(\mathcal{L}_i^T\right)_{i=1,2,3} \leq \frac{1}{15}, \tag{39}$$

where $\mathcal{L}_i^T$ are eigenvalues of $H_{ij}^{(T)}$. Using the axisymmetric relations $H_{11}^{(T)} = H_{22}^{(T)} = -H_{33}^{(T)}/2$, one obtains that the largest eigenvalue is $H_{33}^{(T)}$. Thus, in HITSG, the realizability condition is verified (otherwise one would have negative scalar variance spectra) and the important feature is that the anisotropy reaches its maximal value at large scales in Saffman turbulence.

The case of Batchelor turbulence is a bit different: indeed, because of classical backscatter of energy, strong inverse transfers initiate a return to isotropy mechanism at large scales [7, 21, 37], so that the large scales level of anisotropy can decrease with time (or equivalently can decrease when Re_λ decreases). This is more visible in the case $Pr \ll 1$ because the Péclet number is in general lower than in the case $Pr \gg 1$, as illustrated in figure 9. There, $H_{33}^{(T)}$ for $Pr = 10^{-4}$ is displayed at different times during the decay, or equivalently at various decreasing Reynolds numbers, so that the Péclet number goes from $Pe_\lambda = 193$ down to $Pe_\lambda = 15$. Even though the large scales level of anisotropy remains close to 1/15, it nevertheless slightly diminishes.

5. Conclusion

Decaying homogeneous isotropic turbulence with a mean scalar gradient (HITSG) that sustains scalar fluctuations has been investigated numerically at large Reynolds numbers with the use of a recent anisotropic EDQNM modelling developed by Briard, Gomez and Cambon [7]. The present work is a direct application of the latter spectral modelling in a framework where the Prandtl number is either very small or very large: first, four quantitative comparisons are proposed. The good agreement between the present results and DNS, LES and other models, permits to assess the relevance of the model at $Pr \ll 1$ and $Pr \gg 1$ over a wide range of Reynolds numbers. This notably confirms numerically theoretical spectral scal-

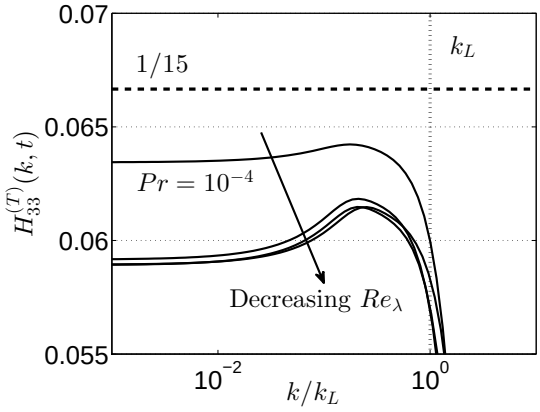

Figure 9. Zoom at large scales for $H_{33}^{(T)}$ in Batchelor turbulence ($\sigma = 4$) for $Pr = 10^{-4}$, along with the integral wavenumber k_L. The four different curves are at $Pe_\lambda = 193$, 87, 36 and 15.

ings for the scalar variance spectrum $E_T(k,t)$ and the cospectrum $\mathcal{F}(k,t)$. Hence, in HITSG, at large Reynolds numbers, it is notably recovered that for $Pr \ll 1$, E_T and $\mathcal{F}$ scale respectively in $k^{-5/3}$ and $k^{-7/3}$ in the inertial-convective range, and then, from the Corrsin-Obukhov wavenumber k_{CO}, in $k^{-17/3}$ and $k^{-11/3}$ in the inertial-diffusive range. Moreover, when $Pr \gg 1$, the k^{-1} viscous convective range beyond k_η for E_T is not modified with the presence of a mean scalar gradient. The assessment of these scalings is one of the main results of the present paper. For both low and large Prandtl numbers, budget terms of the evolution equation of $E_T(k,t)$ were analyzed as well: it was shown that at large scales, the production is always stronger than non-linear transfers. At small scales for $Pr \ll 1$, even at large Re_λ, dissipation is stronger than non-linear transfers: in the limit where the Péclet number tends to zero, dissipation balances production.

Secondly, the time evolution of the scalar variance $< \theta^2 >$ and the mixed-correlation $< u_3\theta >$ was investigated at large Reynolds numbers: it was shown numerically that the theoretical predictions of [7] for the algebraic time exponents are still valid for $Pr \ll 1$ and $Pr \gg 1$, consistently with a similar result for the scalar variance decay in HIT [18]: the Prandtl number does not affect the asymptotic time evolution of $< \theta^2 >$ and $< u_3\theta >$ at large Reynolds numbers, only at moderate ones. This is an important feature: indeed, the algebraic time exponents for $< \theta^2 >$ and $< u_3\theta >$ as functions of the large scales initial conditions were first derived in (BGC), and to assess them for Prandtl numbers strongly different from unity was needed to underline some similarities with HIT. In addition, it was shown numerically that the pressure-scalar correlation $< p\partial_3\theta >$, which is responsible for the destruction of the scalar flux, decays with the same rate as the kinetic energy, independently of the Prandtl number.

Afterwards, the Reynolds and Prandtl numbers dependence of the normalized cospectrum correlation $\rho_{w\theta}$ was addressed as well: the present spectral modelling provides good quantitative results with respect to DNS. Notably, it was found that at a fixed moderate Reynolds number, say $Re_\lambda \sim 100$, $\rho_{w\theta}$ decreases in magnitude when the Prandtl number either increases or decreases, in agreement with the prediction of Yeung and Sreenivasan [17]. The linear dependence of the Nusselt number with the Péclet number is also recovered.

Moreover, it was shown numerically that the small scales of the scalar second-order moments return to isotropy, provided the Péclet number is large enough. This notably implies, for highly diffusive passive scalars, the need to reach very high Taylor Reynolds numbers Re_λ when one wants to obtain a clear $k^{-17/3}$

inertial-diffusive scaling, which numerically requires that $Pr \leq 10^{-3}$.

This numerical work is a direct application of the anisotropic EDQNM modelling developed by Briard, Gomez and Cambon [7] for homogeneous anisotropic turbulence, valid for any mean velocity and mean scalar gradients, which in particular permits to reach very large Reynolds numbers. The main goal of this paper was to show that this spectral model can be used to produce relevant results when the Prandtl number strongly departs from unity. In particular, regimes of either very large Reynolds and Prandtl numbers, or very large Reynolds numbers and very low Prandtl numbers, never reached before in HITSG, were investigated: the consistency of the results over this wide range of parameters constitute an interesting result, both for theoretical considerations, and for practical purposes as well, regarding for instance one-point modelling with the predictions of $< \theta^2 >$, $< u_3\theta >$ and $\rho_{w\theta}$.

Disclosure statement

No potential conflict of interest was reported by the authors.

References

[1] Z. Warhaft, *Passive scalars in turbulent flows*, Annu. Rev. Fluid Mech 32 (2000), p. 203240.
[2] K.R. Sreenivasan, *On local isotropy of passive scalars in turbulent shear flows*, Proceedings: Mathematical and Physical Sciences 434 (1991), pp. 165–182.
[3] C. Tong, and Z. Warhaft, *On passive scalar derivative statistics in grid turbulence*, Phys. Fluids 6 (1994), pp. 2165–2176.
[4] A. Pumir, *A numerical study of the mixing of a passive scalar in three dimensions in the presence of a mean gradient*, Phys. Fluids 6 (1994), pp. 2118–2132.
[5] A. Celani, A. Lanotte, A. Mazzino, and M. Vergassola, *Universality and Saturation of Intermittency in Passive Scalar Turbulence*, Phys. Rev. Lett. 84 (2000), pp. 2385–2388.
[6] W.J.T. Bos, *On the anisotropy of the turbulent passive scalar in the presence of a mean scalar gradient*, J. Fluid Mech. 744 (2014), pp. 38–64.
[7] A. Briard, T. Gomez, and C. Cambon, *Spectral modelling for passive scalar dynamics in homogeneous anisotropic turbulence*, J. Fluid Mech. 799 (2016), pp. 159–199.
[8] L. Danaila, P.L. Gal, F. Anselmet, F. Plaza, and J.F. Pinton, *Some new features of the passive scalar mixing in a turbulent flow*, Phys. Fluids 11 (1999), pp. 636–646.
[9] S. Herr, L.P. Wang, and L.R. Collins, *EDQNM model of a passive scalar with a uniform mean gradient*, Phys. Fluids 8 (1996), p. 1588.
[10] M.R. Overholt, and S.B. Pope, *Direct numerical simulation of a passive scalar with imposed mean gradient in isotropic turbulence*, Phys. Fluids 8 (1996), pp. 3128–3148.
[11] L. Mydlarski, and Z. Warhaft, *Passive scalar statistics in high-Péclet-number grid turbulence*, J. Fluid Mech. 358 (1998), p. 135175.
[12] W.J.T. Bos, H. Touil, and J.P. Bertoglio, *Reynolds number dependency of the scalar flux spectrum in isotropic turbulence with a uniform scalar gradient*, Phys. Fluids 17 (2005).
[13] L. Mydlarski, *Mixed velocity–passive scalar statistics in high-Reynolds-number turbulence*, J. Fluid Mech. 475 (2003), p. 173203.
[14] T. Gotoh, T. Watanabe, and Y. Suzuki, *Universality and anisotropy in passive scalar fluctuations in turbulence with uniform mean gradient*, J. Turb. 12 (2011), pp. 1–27.
[15] P.A. O'Gorman, and D.I. Pullin, *Effect of Schmidt number on the velocityscalar cospectrum in isotropic turbulence with a mean scalar gradient*, J. Fluid Mech. 532 (2005), p. 111140.
[16] W.J.T. Bos, B. Kadoch, K. Schneider, and J.P. Bertoglio, *Inertial range scaling of the scalar flux spectrum in two-dimensional turbulence*, Phys. Fluids 21 (2009), pp. 115105, 1–8.
[17] P.K. Yeung, and K.R. Sreenivasan, *Direct numerical simulation of turbulent mixing at very low Schmidt number with a uniform mean gradient*, Phys. of Fluids 26 (2014), p. 015107.
[18] A. Briard, T. Gomez, P. Sagaut, and S. Memari, *Passive scalar decay laws in isotropic turbulence: Prandtl number effects*, J. Fluid Mech. 784 (2015), pp. 274–303.
[19] M. Lesieur *Turbulence in Fluids*, 4th , Fluid Mechanics and its applications Vol. 84, Springer Netherlands, 2008.
[20] V. Mons, C. Cambon, and P. Sagaut, *A spectral model for homogeneous shear-driven anisotropic turbulence in terms of spherically-averaged descriptors*, J. Fluid Mech. 788 (2016), pp. 147–182.
[21] A. Briard, T. Gomez, V. Mons, and P. Sagaut, *Decay and growth laws in homogeneous shear turbulence*, J. Turb. 17 (2016), pp. 159–199.
[22] M. Meldi, and P. Sagaut, *Further insights into self-similarity and self-preservation in freely decaying isotropic turbulence*, J. Turb. 14 (2013), pp. 24–53.

[23] V. Mons, J.C. Chassaing, T. Gomez, and P. Sagaut, *Is isotropic turbulence decay governed by asymptotic behavior of large scales? An eddy-damped quasi-normal Markovian-based data assimilation study*, Phys. Fluids 26 (2014), p. 115105.
[24] M. Lesieur, and S. Ossia, *3D isotropic turbulence at very high Reynolds numbers: EDQNM study*, J. Turb. 1 (2000), pp. 1–25.
[25] S.B. Pope *Turbulent Flows*, Cambridge University Press, Cambridge, UK, 2000.
[26] A. Briard, and T. Gomez, *Mixed-derivative skewness for high Prandtl and Reynolds numbers in homogeneous isotropic turbulence*, Phys. Fluids 28 (2016), p. 081703.
[27] G. Batchelor, I. Howells, and A. Townsend, *Small-scale variation of convected quantities like temperature in turbulent fluid Part 2. The case of large conductivity*, J. Fluid Mech. 5 (1959), pp. 134–139.
[28] A. Briard, and T. Gomez, *Passive scalar convective-diffusive subrange for low Prandtl numbers in isotropic turbulence*, Phys. Review E 91 (2015), p. 011001(R).
[29] D.D. Marinis, S. Chibbaro, M. Meldi, and P. Sagaut, *Temperature dynamics in decaying isotropic turbulence with Joule heat production*, J. Fluid Mech. 724 (2013), p. 425449.
[30] J.R. Chasnov, *Simulation of the inertial-conductive subrange*, Phys. Fluids A 3 (1991), pp. 1164–1168.
[31] G. Batchelor, *Small-scale variation of convected quantities like temperature in turbulent fluid Part 1. General discussion and the case of small conductivity*, J. Fluid Mech. 5 (1959), pp. 113–133.
[32] C.H. Gibson, *Fine Structure of Scalar Fields Mixed by Turbulence. II. Spectral Theory*, The Phys. Fluids 11 (1968), pp. 2316–2327.
[33] J. Qian, *Viscous range of turbulent scalar of large Prandtl number*, Fluid Dyn. Res. 15 (1995), pp. 103–112.
[34] D. Bogucki, A. Domaradzki, and P.K. Yeung, *Direct numerical simulations of passive scalars with $Pr > 1$ advected by turbulent flow*, J. Fluid Mech. 343 (1997), pp. 111–130.
[35] P.K. Yeung, S. Xu, and K.R. Sreenivasan, *Schmidt number effects on turbulent transport with uniform mean scalar gradient*, Phys. Fluids 14 (2002), pp. 4178–4191.
[36] P.K. Yeung, S. Xu, D.A. Donzis, and K.R. Sreenivasan, *Simulations of Three-Dimensional Turbulent Mixing for Schmidt Numbers of the Order 1000*, Flow, Turbulence and Combustion 72 (2004), p. 333347.
[37] G.L. Eyink, and D.J. Thomson, *Free decay of turbulence and breakdown of self-similarity*, Phys. Fluids 12 (2000), pp. 477–479.
[38] T. Gotoh, and T. Watanabe, *Scalar flux in a uniform mean scalar gradient in homogeneous isotropic steadyturbulence*, Phys. D 241 (2012), pp. 141–148.
[39] A. Gylfason, and Z. Warhaft, *Effects of axisymmetric strain on a passive scalar field: modelling and experiment*, J. Fluid Mech. 628 (2009), p. 339356.
[40] P. Vedula, P.K. Yeung, and R.O. Fox, *Dynamics of scalar dissipation in isotropic turbulence: a numerical and modelling study*, J. Fluid Mech. 433 (2001), pp. 29–60.

Appendix A. Evolution equations of the dissipation rates ϵ_T and $\epsilon_{\mathcal{F}}$

Unlike the scalar variance K_T and the mixed-correlation $K_{\mathcal{F}}$ whose evolution equations are often investigated, the time evolution of their respective dissipation rates ϵ_T and $\epsilon_{\mathcal{F}}$ is less addressed. This is the reason why their general evolution equations are derived here, only using the homogeneity assumption, and are further simplified for HITSG.

The starting point is the equations for the fluctuating velocity and scalar fields u_i and θ, in the presence of both mean velocity and scalar fields U_i and Θ:

$$\left(\frac{\partial}{\partial t}+u_j\frac{\partial}{\partial x_j}\right)u_i+U_j\frac{\partial u_i}{\partial x_j}+u_j\frac{\partial U_i}{\partial x_j}=-\frac{\partial p}{\partial x_i}+\nu\frac{\partial^2 u_i}{\partial x_j\partial x_j},\qquad A_{ij}=\frac{\partial U_i}{\partial x_j}, \tag{A1}$$

$$\frac{\partial\theta}{\partial t}+U_j\frac{\partial\theta}{\partial x_j}+u_j\lambda_j+\frac{\partial}{\partial x_j}(\theta u_j)=a\frac{\partial^2\theta}{\partial x_j\partial x_j},\qquad \lambda_j=\frac{\partial\Theta}{\partial x_j}. \tag{A2}$$

Let's define as well the scalar gradient $\xi_i=\partial_i\theta$, so that one has $\epsilon_T=a<\xi_i\xi_i>$, where we write $<\xi_i\xi_i>=<\xi^2>$. To obtain the general evolution equation of the scalar covariance $<\xi_i\xi_j>$, one needs to derive the evolution equation (A2) of θ with respect to x_i, to multiply it by $\partial_j\theta$, and to sum it with the equation of $\partial_j\theta$ multiplied by $\partial_i\theta$. After ensemble average, this yields in the homogeneous

framework

$$\frac{\partial < \xi_i\xi_j >}{\partial t} + \lambda_l\Big(< \frac{\partial u_l}{\partial x_i}\frac{\partial \theta}{\partial x_j} > + < \frac{\partial u_l}{\partial x_j}\frac{\partial \theta}{\partial x_i} > \Big) + < \frac{\partial \theta}{\partial x_j}\frac{\partial^2 \theta u_l}{\partial x_l \partial x_i} > + < \frac{\partial \theta}{\partial x_i}\frac{\partial^2 \theta u_l}{\partial x_l \partial x_j} >$$
$$+ < A_{li}\frac{\partial \theta}{\partial x_l}\frac{\partial \theta}{\partial x_j} > + < A_{lj}\frac{\partial \theta}{\partial x_l}\frac{\partial \theta}{\partial x_i} > + < U_l\frac{\partial \theta}{\partial x_j}\frac{\partial^2 \theta}{\partial x_i \partial x_l} > + < U_l\frac{\partial \theta}{\partial x_i}\frac{\partial^2 \theta}{\partial x_j \partial x_l} >$$
$$= a\Big[< \frac{\partial \theta}{\partial x_j}\frac{\partial^3 \theta}{\partial x_i \partial x_l \partial x_l} > + < \frac{\partial \theta}{\partial x_i}\frac{\partial^3 \theta}{\partial x_j \partial x_l \partial x_l} > \Big]. \qquad \text{(A3)}$$

This equation can be simplified: first, $< \partial_l(U_l\,\xi_i\,\xi_j) >= 0$ which simplifies the two terms in U_l. Then, using $< \partial_l(u_l\,\xi_i\,\xi_j) >= 0$ simplifies the fourth and fifth terms. Finally, the diffusion terms can be grouped remarking that $< \partial^2_{ll}(\xi_i\xi_j) >= 0$. This yields

$$\frac{\partial < \xi_i\xi_j >}{\partial t} + \lambda_l\Big(< \frac{\partial u_l}{\partial x_i}\frac{\partial \theta}{\partial x_j} > + < \frac{\partial u_l}{\partial x_j}\frac{\partial \theta}{\partial x_i} > \Big) + < \frac{\partial \theta}{\partial x_j}\frac{\partial u_l}{\partial x_i}\frac{\partial \theta}{\partial x_l} > + < \frac{\partial \theta}{\partial x_i}\frac{\partial u_l}{\partial x_j}\frac{\partial \theta}{\partial x_l} >$$
$$+ < A_{li}\frac{\partial \theta}{\partial x_l}\frac{\partial \theta}{\partial x_j} > + < A_{lj}\frac{\partial \theta}{\partial x_l}\frac{\partial \theta}{\partial x_i} >= -2a < \frac{\partial^2 \theta}{\partial x_j \partial x_l}\frac{\partial^2 \theta}{\partial x_i \partial x_l} > . \qquad \text{(A4)}$$

This equation is more simplified than the one given in [39], thanks to $< \partial_l(u_l\,\xi_i\,\xi_j) >= 0$. In the end, the evolution equation of $< \xi^2 >$ in homogeneous turbulence reads

$$\frac{\partial < \xi^2 >}{\partial t} + 2\lambda_j < \frac{\partial u_j}{\partial x_i}\frac{\partial \theta}{\partial x_i} > + 2 < \frac{\partial \theta}{\partial x_i}\frac{\partial u_j}{\partial x_i}\frac{\partial \theta}{\partial x_j} > + 2 < A^+_{ij}\frac{\partial \theta}{\partial x_i}\frac{\partial \theta}{\partial x_j} >$$
$$= -2a < \frac{\partial^2 \theta}{\partial x_i \partial x_j}\frac{\partial^2 \theta}{\partial x_i \partial x_j} >= -2a < \frac{\partial \xi_i}{\partial x_j}\frac{\partial \xi_i}{\partial x_j} > . \qquad \text{(A5)}$$

This equation further simplifies in HITSG where $A_{ij} = 0$ and only $\lambda_3 = -\Lambda$. This yields

$$\frac{\partial < \xi^2 >}{\partial t} = 2\Lambda < \frac{\partial u_3}{\partial x_i}\frac{\partial \theta}{\partial x_i} > -2 < \frac{\partial \theta}{\partial x_i}\frac{\partial u_j}{\partial x_i}\frac{\partial \theta}{\partial x_j} > -2a < \frac{\partial \xi_i}{\partial x_j}\frac{\partial \xi_i}{\partial x_j} >, \qquad \text{(A6)}$$

in agreement with [40].

However, for the evolution equation of $< \partial_j u_i\,\partial_j \theta >$, no references have been found. Here are some details. The process is similar to what was done for $< \xi^2 >$: one needs to derive the evolution equation (A2) of θ with respect to x_j, to multiply it by $\partial_j u_i$, and to sum it with the equation (A1) of u_i derived by x_j and multiplied

by $\partial_j\theta$. This yields

$$\frac{\partial}{\partial t}<\frac{\partial u_i}{\partial x_j}\frac{\partial\theta}{\partial x_j}>+\lambda_j<\frac{\partial u_j}{\partial x_l}\frac{\partial u_i}{\partial x_l}>+A_{ij}<\frac{\partial u_j}{\partial x_l}\frac{\partial\theta}{\partial x_l}>$$
$$+<u_j\frac{\partial\theta}{\partial x_l}\frac{\partial^2 u_i}{\partial x_j\partial x_l}>+<u_j\frac{\partial u_i}{\partial x_l}\frac{\partial^2\theta}{\partial x_j\partial x_l}>+<\frac{\partial u_i}{\partial x_j}\frac{\partial\theta}{\partial x_l}\frac{\partial u_j}{\partial x_l}>+<\frac{\partial u_i}{\partial x_l}\frac{\partial\theta}{\partial x_j}\frac{\partial u_j}{\partial x_l}>$$
$$+A_{jl}\Big(<\frac{\partial\theta}{\partial x_l}\frac{\partial u_i}{\partial x_j}>+<\frac{\partial\theta}{\partial x_j}\frac{\partial u_i}{\partial x_l}>\Big)+<U_j\frac{\partial\theta}{\partial x_l}\frac{\partial^2 u_i}{\partial x_j\partial x_l}>+<U_l\frac{\partial u_i}{\partial x_l}\frac{\partial^2\theta}{\partial x_j\partial x_l}>$$
$$=-<\frac{\partial\theta}{\partial x_l}\frac{\partial^2 p}{\partial x_i\partial x_l}>+a<\frac{\partial u_i}{\partial x_l}\frac{\partial^3\theta}{\partial x_j\partial x_j\partial x_l}>+\nu<\frac{\partial\theta}{\partial x_l}\frac{\partial^3 u_i}{\partial x_j\partial x_j\partial x_l}>. \qquad \text{(A7)}$$

This equation simplifies using similar relations as before, such as $<\partial_j(u_j\partial_l\theta\,\partial_l u_i)>=0$ and $<\partial_l(\partial_l u_i\,\partial^2_{jj}\theta)>=0$, and reads

$$\frac{\partial}{\partial t}<\frac{\partial u_i}{\partial x_j}\frac{\partial\theta}{\partial x_j}>+\lambda_j<\frac{\partial u_j}{\partial x_l}\frac{\partial u_i}{\partial x_l}>+A_{ij}<\frac{\partial u_j}{\partial x_l}\frac{\partial\theta}{\partial x_l}>$$
$$+<\frac{\partial u_i}{\partial x_j}\frac{\partial\theta}{\partial x_l}\frac{\partial u_j}{\partial x_l}>+<\frac{\partial u_i}{\partial x_l}\frac{\partial\theta}{\partial x_j}\frac{\partial u_j}{\partial x_l}>+A_{jl}\Big(<\frac{\partial\theta}{\partial x_l}\frac{\partial u_i}{\partial x_j}>+<\frac{\partial\theta}{\partial x_j}\frac{\partial u_i}{\partial x_l}>\Big)$$
$$=-<\frac{\partial\theta}{\partial x_l}\frac{\partial^2 p}{\partial x_i\partial x_l}>-(\nu+a)<\frac{\partial^2 u_i}{\partial x_l\partial x_l}\frac{\partial^2\theta}{\partial x_j\partial x_j}>. \qquad \text{(A8)}$$

In HITSG, this equation further simplifies into

$$\frac{\partial}{\partial t}\Big(\frac{\epsilon_{\mathcal{F}}}{\nu+a}\Big)=\Lambda\frac{\epsilon}{3\nu}-<\frac{\partial u_3}{\partial x_j}\frac{\partial\theta}{\partial x_l}\frac{\partial u_j}{\partial x_l}>-<\frac{\partial u_3}{\partial x_l}\frac{\partial\theta}{\partial x_j}\frac{\partial u_j}{\partial x_l}>$$
$$+<\frac{\partial p}{\partial x_3}\frac{\partial^2\theta}{\partial x_l\partial x_l}>-(\nu+a)<\frac{\partial^2 u_3}{\partial x_l\partial x_l}\frac{\partial^2\theta}{\partial x_j\partial x_j}>. \qquad \text{(A9)}$$

It seems that such an equation was not derived before: its deeper investigation with DNS may notably provide further information for the improvement of RANS models.